として、遺伝的アルゴリズム（Genetic Algorithm：GA）を用いることとした[1]。GAは、広い設計空間から比較的良好な解もしくは近似解を短時間で探し出せる手法であり、本磁気軸受の設計に適していると考えた。

GAは、何億年もかけて生物が進化してきた遺伝的な法則を、工学的にモデル化したものである。GAの一般的な手順は、先ず初期世代の個体群を生成（初期化）し、設定した目的関数で各個体の適合度を決定する（評価）。ここで、終了条件を満たし、適合度が最大の固体を最適解とする（終了判定）。また、適合度の高い固体はその数を増やし、低いものは淘汰され（選択）、増えた個体間での組み換えを行い新しい個体を生成する（交叉）。さらに、ランダムに選ばれた個体のいずれかの値を適当な別の値に置き換え（突然変異）、評価へと戻る。

GA を基に作成した最適化設計プログラムのフローチャートを Fig.1 に示す。終了条件を、本磁気軸受をポンプとして使用したとき、ロータが 5000 [rpm] 時に受けるスラストカ 24.2 [N]以上の磁気吸引力が発生可能となったときとした（Type1）。また本プログラムにおける制約条件を浮上用の磁束密度および消費電力、磁気軸受の長さおよび直径とし、それぞれ 1.5 [T]、2 [W]、55 [mm]、65 [mm]とした。ここで、本プログラムで用いた計算式では漏れ磁束を考慮していないため、実機が要求する磁気吸引力を発生できないことが示唆される。よって、磁気吸引力において安全率 1.5, 2 をとり、36.3、48.4 [N] 以上の磁気吸引力が発生可能な磁気軸受（Type2、Type3）の最適設計計算も行った。尚、Type2、Type3 では、磁気吸引力を大きくしたため、磁気軸受サイズの制限を、それぞれ 60×70 [mm]、80×80 [mm]とした。

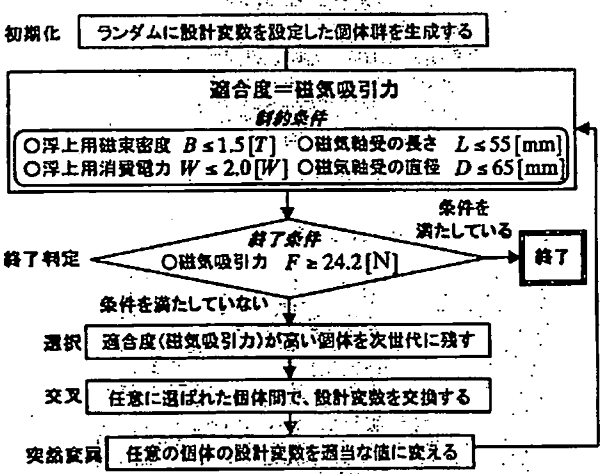

Fig.3 Flow of the optimization design for the magnetic bearing (Type1)

5. 最適化設計計算結果と考察

本プログラムを用いた最適化設計の結果を Fig.4 に示す。結果から、最適方向とは逆方向、つまり条件が緩い方に個体が集まっていることが分かる。さらに、一方が良ければもう一方が悪くなるというパレート解となっている。よって、GA を用いた最適化設計がうまく動作したと言える。

今回、各結果の中で浮上用消費電力が最も低い個体を最適解として選んだ。その設計変数を Table.1 に示す。今後、この結果をもとに、有限要素法を用いた 3 次元磁場解析を行い、求める磁気吸引力が発生可能であるかを確認し、ふさわしいものを実機として製作する。

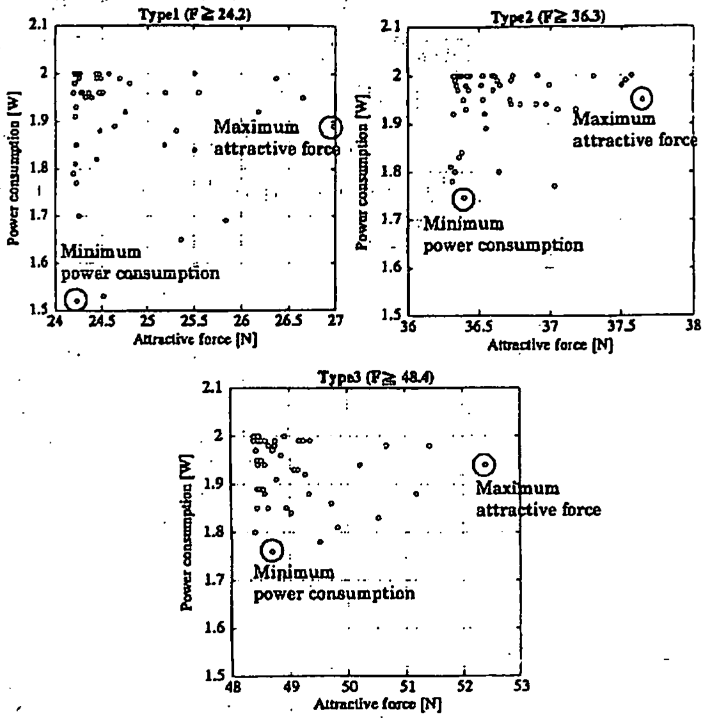

Fig.4 Result of the optimization design with GA

Table.1 Dimension of the magnetic bearing

	Type1	Type2	Type3
Attractive force [N]	24.2	37.1	58.5
Power consumption [W]	1.5	1.76	1.76
Cross sectional area of the permanent magnet [mm^2]	48.5	39.1	39.6
Length of the permanent magnet [mm]	9.9	28.5	17.8
Winding [turn]	155	295	738
Length of the magnetic bearing [mm]	48.3	59.8	76.9
Diameter of the magnetic bearing [mm]	59.9	69.9	76.4

6. 結言

GA を用いた人工心臓用磁気軸受の最適設計法の考案を行った。また、考案した最適設計法を用いて、3 種類の磁気軸受の設計を行った。今後、3 種類の磁気軸受の磁場解析を行い、性能を比較した上で、最良の磁気軸受の製作し、性能評価を行う。

7. 謝辞

本研究の一部は厚生労働科学研究費補助金の支援のもと行われた。

8. 参考文献

[1] 渡辺真也他, 遺伝的アルゴリズムを用いた多目的最適化へのアプローチ, 日本機械学会誌, Vol.106, No.1011, pp49, 2003

高分子材料へのDLC膜の形成とトライボロジー評価
Tribological properties of DLC films deposited on polymers

○松本　良平*, 尾関　和秀**, 平栗　健二***, 福井　康裕***
* 東京電機大学理工学研究科
** 茨城大学工学部
*** 東京電機大学理工学部
Ryohei Matsumoto, Dept of Electric & Computer Engineering, School of Science & Engineering, Tokyo Denki University
Kazuhide Ozeki, Dept. of Mechanical Engineering, Ibaraki University
Kenji Hirakuri, Dept. of Electric & Computer Engineering, Tokyo Denki University
Yasuhiro Fukui, Dept. of Electric & Computer Engineering, Tokyo Denki University

1. まえがき

高分子材料であるポリメタクリル酸メチル(Poly-methylmethacrylate : PMMA)は、表面硬度、耐衝撃性、透明性を有することから、工業材料分野や生体材料分野などに利用されている[1]。また、ポリカーボネート(Polycarbonate : PC)は機械材料、生体材料部品として加工性、耐衝撃性、光透過性が活用されている。しかし、これらの高分子材料は磨耗性、腐食性、熱強度に劣るという欠点がある。一方、ダイヤモンド状炭素(Diamond-like carbon : DLC)膜は、生体適合性、化学的安定性、低摩擦係数に優れた特性を有することから、幅広い分野で応用されている[2]。そこで、本研究では化学的気相成長(Chemical vapor deposition : CVD)法により、DLC膜を保護膜として高分子材料上に堆積した。堆積後、生理食塩水中に試料を浸漬し、耐久性を評価した。さらに、摺動性評価ではBall-on disc試験を用い、溶液中への浸漬前後で高分子材料表面の観察、及びヤング率の測定を行った。

2. 実験

2.1 膜の形成

高分子材とDLC膜との密着性の向上させるために、材料表面の改質(組成変化)を酸素(O_2)プラズマ処理により行った。O_2プラズマは、高周波プラズマ装置(PED-401; ANELVA社製)を用いて発生させた。チャンバー内圧力は13 [Pa]とし、印加電力を250 [W]一定とて2分間、基板の表面改質を行った。その後、メタン(CH_4)ガスを流入し、成膜時間を3分として、DLCコーティングを施した。

2.2 浸漬試験

O_2プラズマ処理を行ったPMMA基板と処理を行っていないPMMA基板に前述のDLC薄膜をコートした。これらの試料と処理を行っていないPMMA基板を浸漬試験に用いた。浸漬試験条件は60 [℃]の生理食塩水に試料を浸し、10日間保持した。上記の試料を3点曲げ試験機を用い、ヤング率の比較を行った。また、光学顕微鏡を用い浸漬前後でのPMMA材料表面の形状変化を観測した。

2.3 Ball-on disc 試験

O_2プラズマ処理を行ったDLC/PMMA, 未処理のDLC/PMMAおよび無垢のPMMAの3種類を用意し、Ball-on disc試験を行った。試料を回転ディスク上にテープで固定させ、回転ディスクを120 [rpm]一定で回転させた。また、回転ディスク上部のアーム先端に摺動面となるステンレス球を設置し、垂直方向に一定負荷で試料上に固定した。摺動実験を2分行った後、試料表面の状態を光学顕微鏡により観察した。

3. 結果および考察

3.1 浸漬試験前後の表面観察

浸漬試験前後で比較した光学顕微鏡像を図1, 2に示す。浸漬前の基板において、図1-(b)では多数のクラックが確認された。これは、PMMA基板に対するDLC薄膜の付着強度が低いためと考えられる。O_2プラズマ処理を行った図1-(c)の場合にはクラックは観測されず、平滑な表面が観測された。一方、浸漬後の基板において、浸漬前に観測されたクラック部分が影響を及ぼした大きなクラックと無数の小さなクラックが観測された(図2-(b))。しかし、O_2処理後DLCを堆積した試料(図2-(c))ではクラックは観測されなかった。これらのことより、浸漬前にできたクラックが大きな膜の剥離の要因になっていることが考えられる。また、O_2プラズマ処理を行うことで、PMMAとDLCの密着性が向上したことにより、強固で良質なDLC膜が堆積したと考えられる。

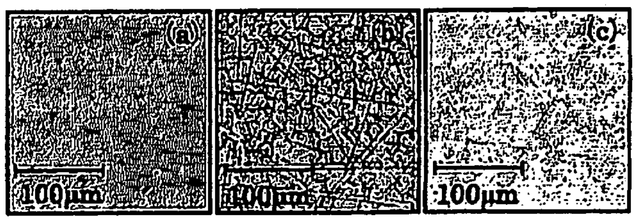

図1　浸漬試験前のPMMA基板
Fig. 1 Micrographs of the samples before the immersion test. (a) PMMA, (b) DLC/PMMA without pre-treatment and (c) DLC/PMMA with pre-treatment.

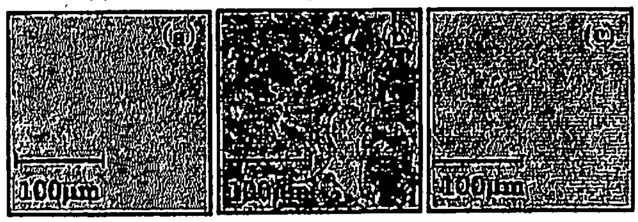

図2　浸漬試験後のPMMA基板
Fig. 2 Micrographs of the samples after the immersion test. (a) PMMA, (b) DLC/PMMA without pre-treatment and (c) DLC/PMMA with pre-treatment.

4. まとめ

プラズマCVD法を用い、高分子材料上にDLCコーティングを施した。その試料を使用し、浸漬試験と*Ball-on disc*試験により耐久性評価を行った。O_2プラズマ前処理を施しDLCコートすることで、PMMA材の生理食塩水に対する耐久性の向上が確認された。また、摺動性試験でも特性の向上が示唆された。

5. 参考文献

(1) 大石不二夫：高分子材料の耐久性, 工業調査会, 1993
(2) 高分子学会高分子表面学会編：高分子表面技術, 1998

TRIBOLOGICAL PROPERTIES OF DLC FILMS DEPOSITED ON DENTAL AND BIOMEDICAL POLYMERS

Ryohei Matsumoto*, Kenji K Hirakuri, Yasuhiro Fukui,
Department of Electric & Computer Engineering, School of Science & Engineering, Ishizuka, Hiki, Hatoyama, Saitama, 350-0394, JAPAN
Tel: +81 492 96 2911 ext 3102, Fax: +81 492 96 6413 Email: ma0731@ff.f.dendai.ac.jp
and Kazuhide Ozeki
Department of Mechanical Engineering, Ibaraki University, 4-12-1, Nakanarusawa, Hitachi, Ibaraki, 316-8511 JAPAN

***Keyword:** Diamond-like carbon, r.f. plasma CVD, PMMA, UHMWPE, polycarbonate, thickness*

ABSTRACT

Diamond-like carbon (DLC) films were coated on high-polymer materials and we evaluated the durability by an immersion test. In addition, we carried out a Ball-on disk test for the tribological evaluation. After the immersion test, the bending moment and Young's modulus values were measured using a three points bending test machine. In the immersion test, the DLC film was detached from the PMMA without the pre-treatment , whereas, there was no deterioration on the PMMA with the pre-treatment. In the ball-on disk test, some scratch traces can be seen on the PC without pre-treatment, whereas, there is no scratch trace on the PC with pre-treatment.

INTRODUCTION

Poly-methylethacrylate (PMMA) has been used for contact lenses and denture teeth because of its various advantages, such as high light transmission, light weight and lower susceptibility to fracture. Polycarbonate (PC) also has good characteristics such as an impact resistance, thermal durability (up to 190 ℃) and optically transparent in a wide spectral region [1, 2]. However, these materials demonstrate low hardness, low resistance to abrasion and poor chemical attack.

On the other hand, DLC films have many superior properties such as extreme hardness, low friction coefficients, chemical inertness and high-corrosion resistance. Since chemical vapor deposition (CVD) technique under room temperature, CVD method is widely used for DLC deposition on polymeric materials.

The DLC coated samples were immersed in the acid solution for estimation of the durability. In addition, the tribological measurement was achieved by ball-on disk test and bending moment and Young's modulus values were obtained.

EXPERIMENTAL PROCEDURE

Sample preparation

PMMA plates (Yamahachi Dental Mfg., Aichi, Japan) and PC (Takiron Mfg., Hyogo, Japan) were cut into 0.8 × 0.8 × 1.0 mm^3 pieces using a diamond cutter.

The Oxygen plasma pre-treatment of the polymer substrate and the deposition of the DLC were performed in an ANELVA PED-401 radiofrequency plasma CVD system. Oxygen plasma pre-treatment was for improving the adhesion strength of the substrate to the deposited DLC films. The substrates were cleaned in H_2O by an ultrasonic washing machine for 10 min before deposition. Half of the samples received plasma pre-treatment before DLC deposition. For this, the gas pressure was keep at 13 Pa and r.f. power was fixed at 250 W. The pre-treatment time was kept constant at 2 min.

For DLC coating, high purity methane (CH_4) gas (99.9999 %) was introduced into the chamber as a reactive gas. The coating was carried out at 13 Pa and 250 W. The deposition time was 3 min to keep the coating thickness at 0.1 μm. The temperature of the substrate remained below 100 °C during the deposition process.

Immersion test

The three kinds of substrates were used for the test. The substrates were the PMMA substrate, the DLC coated substrate without Oxygen pre-treatment, the DLC coated substrate with Oxygen pre-treatment. These samples was immersed in 30 ml of normal saline solution 0.9 % at 60 ℃ for 10 days. Subsequently, the Young's modulus of the immersed substrates were measured using three point bending machine. The substrate surfaces were observed using optical microscope before and after the immersion.

Ball-on disk test

Wear testing was performed using a ball-on-disc apparatus. The lower rotating disc slides against an upper stationary stainless steel ball (316 L; 10 mm in diameter). The used substrates were the DLC coated PMMA and PC with and without the Oxygen pre-treatment. Each substrate was fixed onto the lower rotating disc. The rotating speed was 132 rpm. A normal load of 100 mN was applied to the ball. The test was carried out for 2 min in room-air with humidity up to 35 %.

After the sliding test, optical microscopy was used to observe the morphology of the surface.

RESULTS AND DISCUSSION

Surface observation after the immersion test

Figure. 1 and 2 show the photographs of sample surfaces using the optical microscope before and after the immersion. DLC film deposited the PMMA without the pre-treatment showed many crack (Fig. 1-(b)), whereas there were no cracks in the DLC-coated PMMA with the pre-treatment (Fig. 1-(c)). After the immersion, the film was detached from the PMMA without the pre-treatment (Fig. 2-(b)), whereas, there was no deterioration on the PMMA with the pre-treatment (Fig. 2-(c)). This suggests that the strength of adhesion of the DLC film to PMMA was increased by the Oxygen plasma pre-treatment.

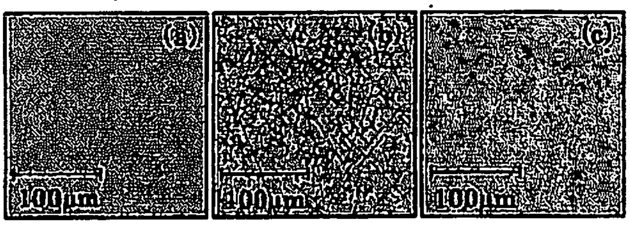

Fig. 1 Micrographs of the samples before the immersion test. (a) PMMA, (b) DLC/PMMA without pre-treatment, (c) DLC/PMMA with pre-treatment.

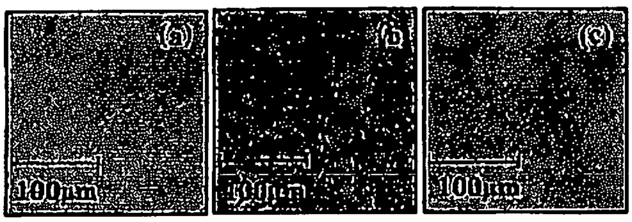

Fig. 2 Micrographs of the samples after the immersion test. (a) PMMA, (b) DLC/PMMA without pre-treatment, (c) DLC/PMMA with pre-treatment.

Measurement of Young's modulus values

Young's modulus values were measured using a three points bending test machine. The DLC/PMMA with pre-treatment showed highest Young's modulus values in all samples.

Surface observation of the samples after the ball-on disk test

Fig. 3 shows the micrographs of the samples after the ball-on disk test. In the PMMA substrate, there was no difference on the surfaces between with and without the pre-treatment. In the PC substrate, some scratch traces can be seen on the PC without pre-treatment (Fig.3-(c)), whereas, there is no scratch trace on the PC with pre-treatment (Fig.3-(d)). These results also indicate that the oxygen plasma pre-treatment can improve the adhesion strength of the DLC film to PC.

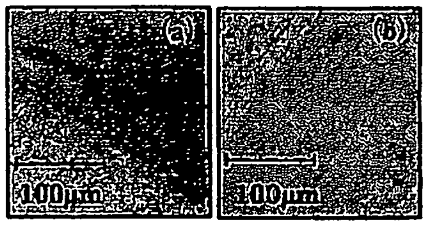

(a) DLC/PMMA with pre-treatment, (b) DLC/PMMA without pre-treatment.

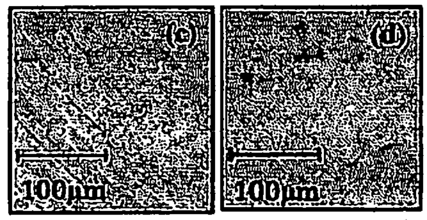

(c) DLC/PC with pre-treatment, (d) DLC/PC without pre-treatment.

Fig 3. Micrographs of the samples after the ball-on disk test.

CONCLUSIONS

DLC films were coated on high-polymer materials (PMMA, PC) and we evaluated the durability by the immersion test and the ball-on disk test. In the immersion test, the DLC film was detached from the PMMA without the pre-treatment, whereas, there was no deterioration on the PMMA with the pre-treatment. In the ball-on disk test, some scratch traces can be seen on the PC without pre-treatment, whereas, there is no scratch trace on the PC with pre-treatment.

ACKNOWLEDGMENTS

This work was partially supported by the frontier research center, Tokyo Denki University.

REFERENCES

[1] N. K. Cuong, et al, Surface and Coatings Technology 174-175 (2003) 1024-1028.

[2] Ali Alanazi et al, Airtificial Organs 24 (8) : 624-627, Blackwell Science, Inc.

TRANSACTIONS ON ELECTRICAL AND ELECTRONIC ENGINEERING
IEEJ Trans 2006; 1: 188–193
Published online in Wiley InterScience (www.interscience.wiley.com). DOI:10.1002/tee.20037

Paper

Characteristics of a Two-dimensional Integrated Magnetic Sensor for Position Sensing and Motor Control

Takayuki Kimura,*[a] Member
Keigo Takasaki,* Member
Toru Masuzawa,** Member

Two-dimensional integrated magnetic sensors for position sensing were designed and fabricated with the standard 0.35-μm CMOS process on silicon. One such type is the n-type Hall sensor that uses an inversion layer under the gate oxide of the MOSFET. The Hall sensors were arrayed (64 × 64), and the control digital circuits and output amplifier were also integrated into the same chip. 'One pixel' was 50 × 50 μm, and the entire chip was 4.9 × 4.9 mm. The sensitivity of one of these sensors was 2.7 mV/(mA·kG). The two-dimensional magnetic flux distribution was measured from the 5-mm diameter Nd–Fe–B rare-earth permanent magnet. About 42 s was required to measure one frame. The position of the magnet could be detected with the fabricated sensors. Magnetic sensors using an inversion layer in MOSFETs are useful for position sensing systems, but their noise characteristics, such as poor sensitivity, should be improved. © 2006 Institute of Electrical Engineers of Japan. Published by John Wiley & Sons, Inc.

Keywords: hall sensor, CMOS, two-dimensional magnetic field, position sensor

Received 25 August 2005; Revised 3 April 2006

1. Introduction

The position sensors used to control motors and actuators in robots or medical tools need to be extremely precise. Although there are various types of position sensors, magnetic field sensors are usually used for reasons of price and size. Several magnetic field sensors are needed to accurately detect the position of an object. Magnetic field sensors are conventionally fabricated with InSb and GaAs, using the Hall effect, because of their high-sensitivity that corresponds to high-mobility. However, it is difficult to achieve compact and highly accurate positioning systems with sensors using such materials.

In contrast, Si is not used to fabricate magnetic field sensors because of its poor sensitivity and mobility. However, Si has demonstrated its superiority in integrated circuits [1]. Integrated circuit technology can overcome faults in silicon characteristics and poor sensitivity with an amplifier and analog signal processing. Si magnetic field sensors show poor sensitivity, but it does not mean the noise floor is high. By using a low-noise amplifier, effective sensitivity can be made comparable to that of InSb and GaAs. Si is also useful in integrating analog and digital systems. Control and signal processing circuits also can be integrated on magnetic field sensors.

We fabricated two-dimensional integrated magnetic field sensors using the Hall effect in Si for sensing position, slant, and rotation. This sensor will be applied to sense the position and to control a magnetic levitated motor with only one sensor. We discuss their fundamental characteristics in this paper.

2. Principles of the Hall Sensor using Inversion Layer in MOSFETs

Magnetic field sensors are made in bulk from InSb and GaAs using the Hall effect. Because Si is not as sensitive

[a] Correspondence to: Takayuki Kimura, Department of Systems Engineering, Ibaraki University, 4-12-1, Nakanarusawa, Hitachi, Ibaraki 315-8511, Japan. E-mail: tkimura@mx.ibaraki.ac.jp
* Faculty of Engineering, Department of Systems Engineering, Ibaraki University, 4-12-1, Nakanarusawa, Hitachi, Ibaraki, 316-8511, Japan
** Faculty of Engineering, Department of Mechanical Engineering, Ibaraki University, 4-12-1, Nakanarusawa, Hitachi, Ibaraki, 316-8511, Japan

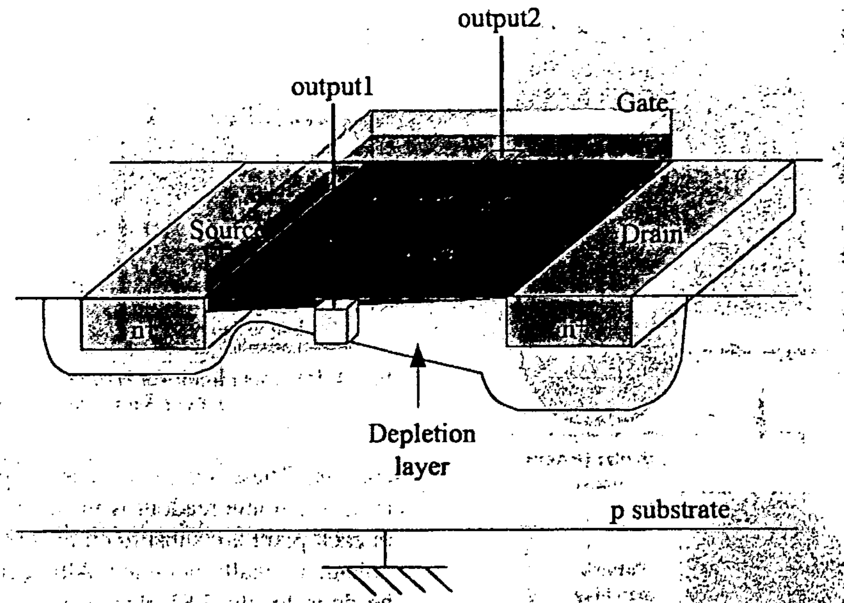

Fig. 1 Cross section of the hall sensor using inversion layer in MOSFET

as InSb and GaAs, it cannot be used utilizing this effect in bulk. A magnetic field sensor using an inversion layer in the MOSFET (Metal-Oxide- Semiconductor Field Effect Transistor) had been proposed [2]. Its configuration is in Fig. 1.

It is similar to an n-channel MOSFET. Only two diffusion regions (marked 'output1' and 'output2' in Fig. 1) are made in the same process with the drain and source added to the other sides of source and drain. These regions are used for the probes to detect the voltage differences in the inversion layers. The Hall effect on the carriers, i.e. electrons in this case, in the inversion layer creates a voltage difference between the probes. This difference changes linearly with the strength of magnetic flux density as

$$V_H = \frac{R_H \cdot I \cdot B}{d} \quad (1)$$

where R_H is the Hall coefficient, I is the current through the inversion layer, B is the magnetic flux density, and d is the thickness of the inversion layer.

The main advantage of this sensor is that it is extremely sensitive because of the thin inversion layer. The mobility in the inversion layer is lower than that of bulk, but its thinness overcomes that fault. The end result is that it is more sensitive than a magnetic field sensor using bulk Si.

3. Principles of Position Sensing and Structure of the Position Sensor

3.1. Concepts Position sensing is done by the measurement of magnetic flux density from a magnet that is placed on the object that we measure or control the position of. Figure 2 shows an example how to detect the position of a motor axis. In this example, a magnet is attached to the edge of a motor axis. A two-dimensional magnetic sensor is placed below this magnet without being in contact. Magnetic flux flows from the magnet. The two-dimensional magnetic sensor will output a voltage proportional to the strength of magnetic flux density. This sensor can get the distribution of the magnetic flux density. Essentially, magnetic flux density from a column-shaped magnet will spread radially. So, 'the image' of magnetic flux density from the two-dimensional magnetic sensor will be a stack of concentric circles of the same voltage. The readout image is already the object in signal processing. Figure 3 shows the signal processing diagram of how the position can take the

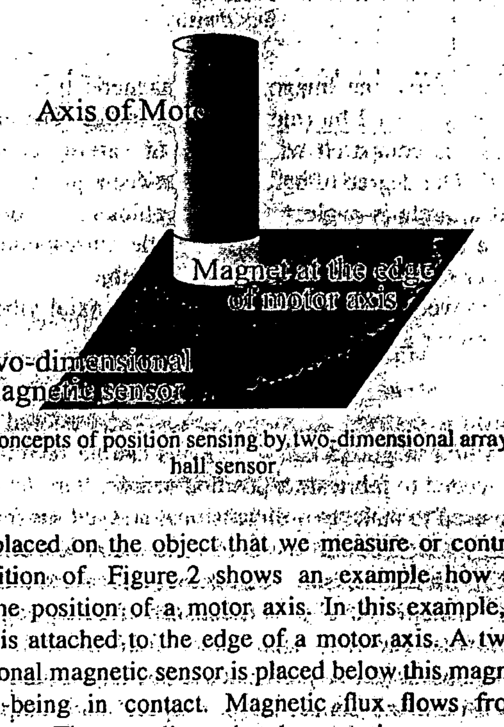

Fig. 2 Concepts of position sensing by two-dimensional arrayed hall sensor

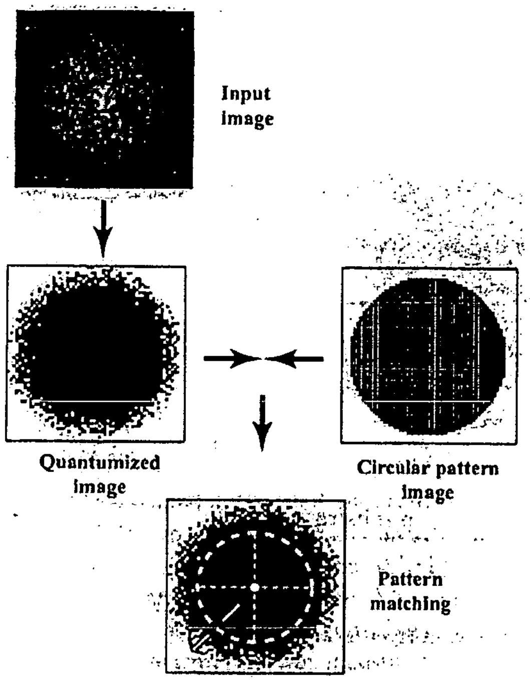

Fig. 3 Method of position sensing from the image of magnetic flux density

image. First, the image of the magnetic flux density is quantized to a 2-bit (monochrome) image. The quantized image is compared with circles of varying centers and radii. The degree of agreement between quantized image and a circle is evaluated by a coefficient of correlation. As a result, the center of the circle corresponds to the center of the magnet attached to the object. For example, the movement of the center shows the axial vibration of the motor as shown in Fig. 2.

3.2. Structure of the readout circuits and data-readout instructions The two-dimensional integration of a magnetic field sensor, as can be seen in Fig. 1, is needed to fabricate a position sensor. Various methods are used to make two-dimensional arrayed sensors. From these, we chose the one used to fabricate the circuit of a CMOS image sensor. The readout circuit for reading the Hall voltage is in Fig. 4. It consists of a two-stage source follower. The first-stage source follower is in a pixel, and consists of two p-channel MOSFETs. Both p-channel MOSFETs are connected to 'output1' and 'output2' and read the Hall voltage alternately. This instruction loses time, but saves area on the LSI (large-scale integration) chip. The second-stage source follower is located in each column and consists of n-channel MOSFETs with an active load.

Signals in one horizontal line from the Hall magnetic field sensors are read at the same time in parallel columns. As the Hall voltage is the difference between 'output1' and 'output2', readout is done twice from each pixel. Then, readout is done sequentially from each

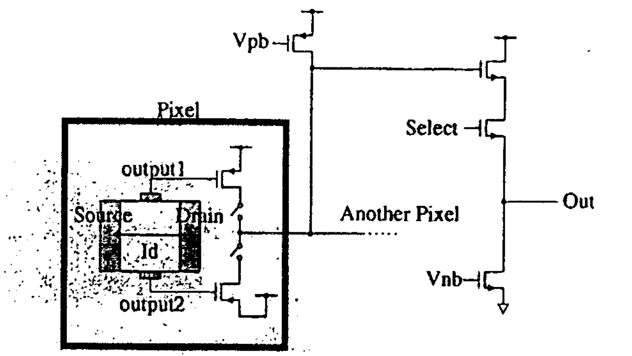

Fig. 4 Readout circuit for Hall voltage. This is one arrangement for CMOS image sensors

column. These instructions are repeated in every row, until one frame readout is finished. The two read signals in each pixel are substituted for each other, and the Hall voltage is finally obtained. Although this calculation can be done by the LSI chip, we did it on a PC (personal computer).

3.3. Two-dimensional magnetic field sensor LSI design The two-dimensional integrated magnetic field sensor was designed for the 2-poly 3-metal standard 0.35-μm CMOS process by Rohm Co., Ltd. The fabricated two-dimensional magnetic sensor is shown in Fig. 5. The control logic circuit for timing generation and the output buffer circuit were also integrated on the same chip of the two-dimensional magnetic field sensor. This integration of the sensor and the other logic circuits is the advantage of the silicon process. This advantage contributes to miniaturization of the device. The dimensions of the LSI chip were 4.9 × 4.9 mm and the pixel size was 50 × 50 μm. The sensing area was 3.2 × 3.2 mm. The magnetic field sensors and output buffer circuit were fully custom-designed by Cadence Virtuso, and the control logic circuits in the Verilog-HDL by Synopsys Design Compiler.

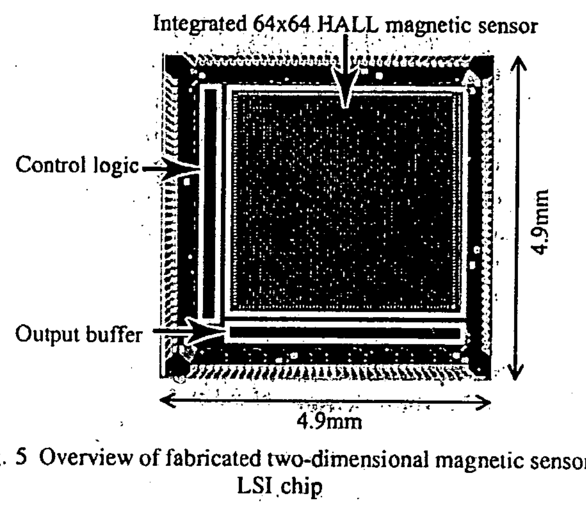

Fig. 5 Overview of fabricated two-dimensional magnetic sensor LSI chip

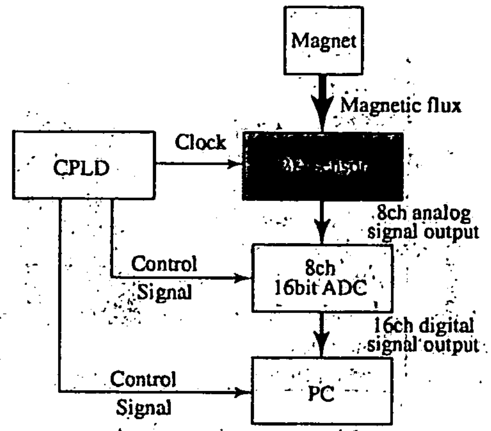

Fig. 6 Block diagram of the measurement system

4. Measurement Results for the Magnetic Field Sensor

4.1. Measurement The magnetic field for the input of the two-dimensional magnetic field sensor was provided by a 5-mm diameter Nd–Fe–B rare-earth permanent magnet. The strength of magnetic flux density was changed by the distance between the magnet and the two-dimensional magnetic field sensor. Figure 6 shows the block diagram of the measurement system. The output Hall voltage from the magnetic sensors was read out as 8-channel analog signals. These signals were converted to digital signals at the same time by eight 16-bit ADCs. Finally, digitized Hall voltage signals were read into the PC. The digitized signals were reconstructed into a two-dimensional image of magnetic field distribution.

The output signal from the fabricated magnetic sensors was very small and its magnitude was a few millivolts. As such a small signal is easily influenced by noise, digital signal averaging was done to remove random noise. For example, Fig. 7 shows the image with averaging 16 times, but this averaging was not sufficient. Averaging 128 times was sufficient to remove random noise from the Hall signals. This averaging suppresses the random noise to −42 dB, but 42 s was needed to average one image. Signals needed to be amplified to reduce noise and measurement time. All magnetic field distribution images in this paper were obtained with 128 times averaging. By the limitation of output voltage level, readout time is very slow. But, potentially, the digital readout drive circuit is strong, and few thousand frames per second readout rate will be achieved if the level of the output voltage is increased.

4.2. Results and discussion Figure 8 plots the results of the relationship between input magnetic flux density and output Hall voltage. This graph shows the average for four different magnetic sensors. The

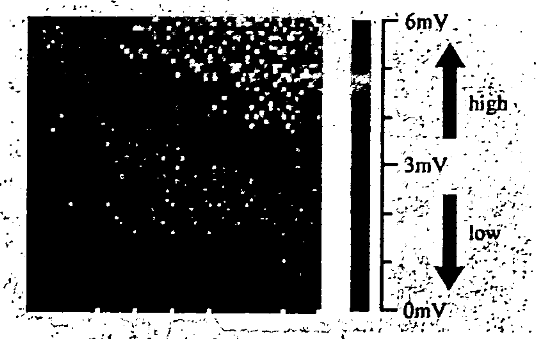

Fig. 7 Noisy image with 16 times averaging

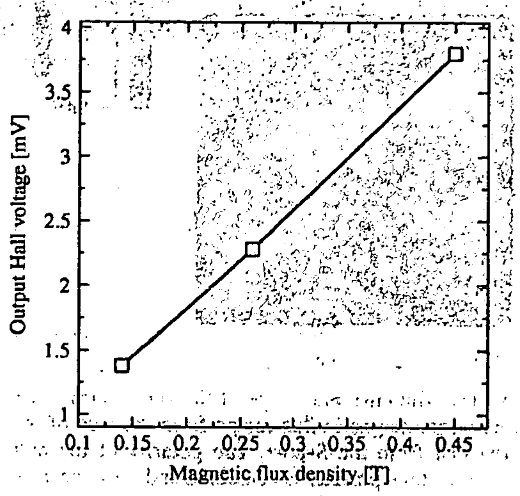

Fig. 8 Relationship between strength of the input magnetic flux density and the output hall voltage

sensitivity calculated from Fig. 8 was 2.7 mV/mA·kG. These sensors are less sensitive than the ones made with InSb and GaAs by two or three figures, but as previously mentioned, signal amplification can boost this low sensitivity. There is good linearity between the input magnetic field and the output voltage.

Figure 9 shows reconstructed two-dimensional magnetic flux distribution images. The shape of the magnet can be recognized. Figure 9(a) is a magnetic flux distribution image from the side of the N-pole and (b) that from the S-pole. Here, voltage polarity has been neglected and only the absolute Hall voltage has been represented; however, the output polarity of the Hall voltage reverses between the magnetic flux from the N- and S-poles. Essentially, a magnetic sensor using the Hall effect can sense the direction of the magnetic flux. The two-dimensional magnetic field sensor we fabricated could also detect the direction of the magnetic flux.

Figure 10 plots a horizontal one line profile of the Hall voltage. This graph corresponds to the top horizontal line in the magnetic flux distribution image of Fig. 9(a). Noise can be seen. This corresponds to the fixed pattern noise caused by the characteristic fluctuation of the MOSFET

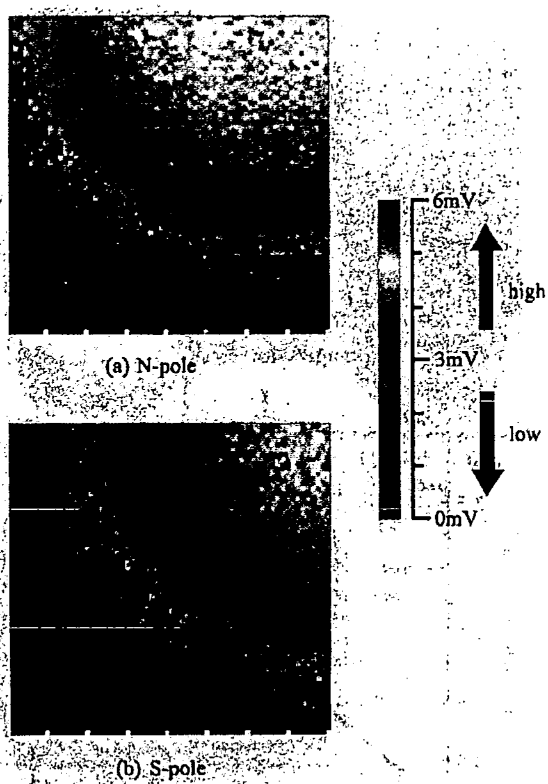

Fig. 9 Two-dimensional image of the Hall voltage distribution. (a) represents magnetic-flux image from the side of the N-pole, and (b) that from the S-pole. The polarity of the hall voltage reverses. Voltage polarity is neglected and only the absolute hall voltage is represented

used in the source followers at each column, but the magnet position can be distinguished by the magnetic flux distribution.

5. Conclusions

Two-dimensional integrated magnetic sensors were designed and fabricated with the standard 0.35-μm CMOS process on silicon. The Hall sensors were arrayed (64 × 64), and the control digital circuits and output buffer were also integrated onto the same chip. The sensitivity of one of these sensors was 2.7 mV/mA·kG. The two-dimensional magnetic field distribution was measured from the 5-mm diameter Nd–Fe–B rare-earth permanent magnet with 128 times averaging. About 42 s was required to measure one frame. The magnetic flux distribution was obtained as a bitmap image. The position of the magnet could be detected with the fabricated sensor. Magnetic sensors using an inversion layer in MOSFETs are useful for position sensing systems, but their noise characteristics, such as poor sensitivity, should be improved.

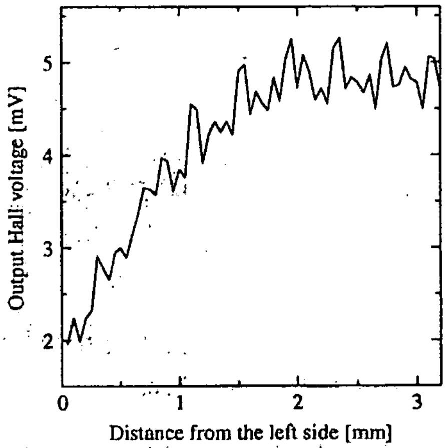

Fig. 10 Horizontal one-line profile of a magnetic field sensor

Acknowledgements

This work was supported by the VLSI Design and Education Center (VDEC) of the University of Tokyo in collaboration with Synopsys, Inc and Cadence Design Systems, Inc. The VLSI chip in this study was fabricated in the chip fabrication program of the VDEC in collaboration with Rohm Corporation and Toppan Printing Corporation. Moreover, this work was partially supported by JSPS Core University Program and the Health and Labor Sciences Research Grants.

References

(1) Nakano Kazuhiro, Takahashi Toru, Kawahito Shoji. A CMOS smart rotary encoder using magnetic sensor arrays. *Proceedings of IEEE Sensors* 2003; 1:206–209.
(2) Gallagher RV, Corak WS. A metal-oxide-semiconductor (MOS) hall element. *Solid State Electronics* 1966; 9:571–580.

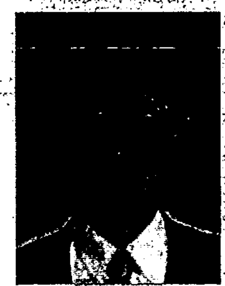

Takayuki Kimura (Member) received the BS and MS degrees in electrical and electronic engineering and PhD degree in electronic and information engineering from Toyohashi University of Technology in 1993, 1995 and 1998, respectively. In 1998, he joined Ibaraki University as a research associate in Systems Engineering and began research in solid-state imaging and systems. Since 2005, he has been an Associate Professor. His major interests are crystal growth, solid-state imaging devices, digital image processing, and their system integration. He is also a member of the Institute of Image Information and Television Engineers and IEEE.

Keigo Takasaki (Non-member) received the BE degree in systems engineering from Ibaraki University, Ibaraki, Japan, in 2004, and is now majoring in Systems Engineering at Ibaraki University Graduate School of Science and Engineering. He is studying and researching LSI technology and design methods of analog integrated circuits. The theme of his research is the development of magnetic sensor systems using standard CMOS technology and digital signal processing.

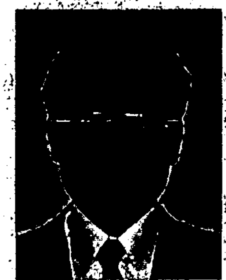

Toru Masuzawa (Member) received the BS, MS, and PhD degrees in Applied Systems Engineering from Tokyo Denki University, Tokyo, Japan, in 1982, 1984, 1991, respectively. From 1987, he was a research assistant in the Department of Precision Mechanical Engineering at the University of Tokyo, Tokyo, Japan. From 1990 to 1997, he was a research associate and a division head of the Department of Artificial Organs at the National Cardiovascular Center Research Institute, Osaka, Japan. In 1998, he moved to Ibaraki University, Hitachi, Japan, as an Associate Professor in the Department of Mechanical Engineering. Since 2002, he has been a professor in that department. His major is Bio-medical Engineering. Especially, he has been working in the field of the artificial heart since 1990 and his current interest is in the magnetically suspended motor for the artificial heart. He is a member of IEEE, the Japan Society of Mechanical Engineers, the Institute of Electrical Engineers of Japan, and a councilor of the Japanese Society for Artificial Organs, Japanese Society for Medical and Biological Engineering, and a member of the Board of Trustees of the International Society for Rotary Blood Pump and The Society of Life Support Technology.

PA01　集積化磁気センサにおけるホール素子の構造改善による出力向上

Improvement of Output of Two-Dimensional Integrated Magnetic Sensor by Optimizing the Structure of Sensor Probe

○石沢　泰輔　，　高崎　慶吾　，　木村　孝之　，　増澤　徹　(茨城大学)

○Taisuke ISHIZAWA，　Keigo TAKASAKI，　Takayuki KIMURA，　Toru MASUZAWA　(Ibaraki University)

1．はじめに

現在、モーターの制御に広く使われている磁気センサには InSb, GaAs などの材料を用いたホール素子が使われているが、これらの素子で正確な位置計測を行うには複数個必要であるためコストや面積などの面で問題になる。そこで MOSFET の反転層を利用した磁気センサを Si 上に二次元に集積化し、磁束分布図を元に位置計測を行う研究を進めている。しかし、Si を用いたホール素子は反転層や増幅回路を併用しても InSb や GaAs と比べ、出力が低くなってしまう。

本研究では集積化磁気センサのホール素子の構造改善による出力向上を目的とした。

2．反転層を利用したホール素子

本研究で使用した磁気センサの構造を図 1 に示す [1]。このホール素子では、n チャネル MOS トランジスタの反転層を形成する電子に対して、ホール効果を起こし、ソース・ドレインに直交する出力端子 (R, S) によってホール電圧 V_H を測定する。ホール素子で発生するホール電圧は、次式で表される。

$$V_H = \frac{R_H \cdot I \cdot B}{d} \quad (1)$$

ここで、V_H はホール電圧、I はチャネルを流れる電流、B はホール素子にかかる磁束、d は素子の厚さ、R_H はホール係数である。MOS トランジスタの反転層は InSb や GaAs のホール素子よりも薄いため高い出力を得やすく、増幅器と共に集積化できる。

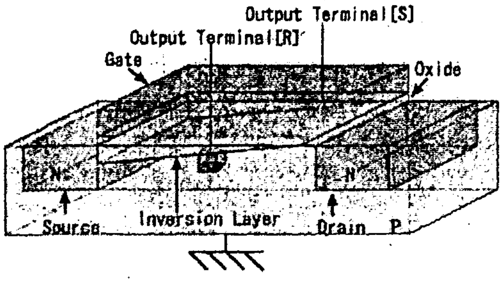

図 1 反転層を利用した磁気センサ

3．ホール素子の構造変更

ソースからドレインへ電子が流れる間、ローレンツ力はかかり続けるので、ドレインに近づくほど電子は曲げられながら進むと考えられる。それにより、ソース近傍とドレイン近傍で電子の挙動が異なるため、出力端子 (R, S) の位置によって出力されるホール電圧 V_H の値が変わると予想できる。よって、端子の位置を変更したホール素子で測定を行った。

今回測定に用いた集積化磁気センサチップは Rohm 社 0.35μm 標準 CMOS プロセスで作製された。チップの一部のホール素子を図 2 に示すように端子位置を変更し作製した。図 2 は左側をソース、右側をドレインとしており、④が従来の端子位置のホール素子である。

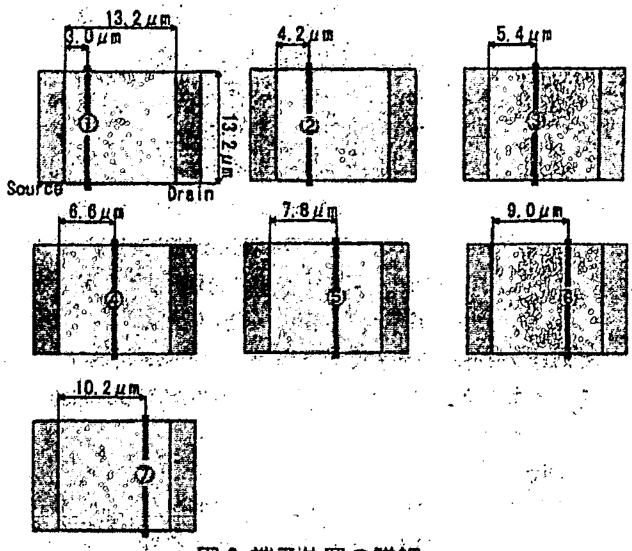

図 2 端子位置の詳細

5．出力の比較と考察

従来の端子位置を基準とした出力電圧比を表 1 に示す。表 1 の端子位置は図 2 の番号に対応したものになっている。

表 1 端子位置を変更したホール素子の出力電圧比

端子位置	①	②	③	④	⑤	⑥	⑦
出力電圧比[%]	0.72	0.80	0.90	1.00	1.09	1.20	1.23

端子位置がソース近傍からドレイン近傍に近づくほど出力電圧が向上し、最大約 20%の出力向上が達成できた。このことからローレンツカにより、ソース近傍と比べてドレイン近傍の電子の分布に大きな偏りが生じていると言える。

5．まとめ

端子位置を変更した磁気センサで測定を行った結果、端子位置をドレイン近傍へ変更することで最大約 20%の出力電圧向上が可能であることがわかった。これにより集積化磁気センサのホール素子の構造改善による出力向上が達成できた。

謝辞　本研究の一部は厚生労働科学研究費補助金によって行われた。本チップ試作は東京大学大規模集積システム設計教育研究センターを通しローム株式会社、凸版印刷株式会社、ケイデンス株式会社およびシノプシス株式会社の協力で行われた。

文献

[1] R. V. GALLAGHER and W. S. CORAK
"A METAL-OXIDE-SEMICONDUCTOR (MOS) HALL ELEMENT",
Solid-State Electronics, Vol. 9, 1966, pp. 571-580.

2007年3月23日（金）　社団法人映像情報メディア学会技術報告
ITE Technical Report Vol.31,No.21,PP. 5 ～ 8
IST2007-21,CE2007-22(Mar.2007)

二次元集積化磁気センサのホール素子構造の改善

†石沢　泰輔　†高崎　慶吾　†木村　孝之　‡増澤　徹

茨城大学大学院　理工学研究科　†システム工学専攻　，‡機械工学専攻
〒316-8511 茨城県日立市中成沢町 4-12-1

E-mail: †06nm904g@hcs.ibaraki.ac.jp

あらまし　一つの磁気センサチップでモーターを制御することを目的に，MOSFET の反転層をホール素子として利用した磁気センサを Si ウエハ上に二次元に集積化した磁気センサを試作した。その結果，磁束を面で測定できるようになった．また，出力電圧を向上させるためにダイナミックドライブ駆動方式を導入し，モーター制御に必要な 1000frame/sec の読み出し速度を達成した．さらに出力電圧を向上させるために，磁気センサの構造を変更した素子の動作検証を行った．その結果，出力電圧を 20%増加することができた．

キーワード　磁気センサ　，　反転層　，　CMOS　，　ホール素子

Improving the sensor output by modifying the structure of Hall sensor of a two-dimensional integrated magnetic sensor

Taisuke Ishizawa　Keigo Takasaki　Takayuki Kimura　Tohru Masuzawa

Graduate School of Science and Engineering, Ibaraki University
4-12-1 Nakanarusawa-cho , Hitachi City , Ibaraki 316-8511

E-mail: †06nm904g@hcs.ibaraki.ac.jp

Abstract The research for controlling of a motor with a tow-dimensional integrated magnetic sensor which was designed and fabricated standard 0.35 μ m CMOS process has been performed. A type of magnetic sensor is Hall sensor using inversion layer under gate oxide of MOSFET. Magnetic field with a two-dimension magnetic sensor was successfully measured. Improving output voltage and reading speed of 1000frame/sec was achieved by the dynamic drive method. As the result, 20% improvement of sensor output voltage with new structure of Hall sensor was obtained.

Keyword Magnetic sensor　,　inversion layer　,　CMOS　,　Hall sensor

1.はじめに

磁気センサは人間の感覚器官で検知できない磁界の大きさ・向きを計測することを目的としたセンサである．半導体を用いた磁気センサにはホール素子があり，一般的に GaAs や InSb が用いられる．しかし，従来のバルクを用いたホール素子では正確なモーターの制御の際に複数個必要であるためコストや設置場所などの面が問題になる．そこで，MOSFET の反転層をホール素子として利用した磁気センサを Si ウエハ上に二次元に集積化することにより磁束を面でとらえ，コスト削減や省スペース化を実現する研究が進められている．

しかし，MOSFET の反転層を利用し，増幅回路を併用しても Si を用いた磁気センサの出力電圧は従来の GaAS や InSb を用いた磁気センサと比べて小さい．ダイナミックドライブ方式を導入することにより出力電圧を向上させ，モーター制御に必要な 1000frame/sec の読み出し速度は達成することができたが，ノイズの影響を大きく受けていた．

本研究では，集積化磁気センサの構造を改善することによりセンサの出力電圧を向上させることを目的とする．

2. 磁気センサチップ

2.1.MOSFET を用いた磁気センサ

電子は正孔と比べ移動度が高いので，n チャネル MOSFET の方が p チャネル MOSFET と比べて流れる電流が大きい．ゲートにしきい値電圧以上の電圧 V_G を印加すると p 型半導体表面の酸化膜界面付近に電子が発生し，反転層を形成する．この反転層がソース・ドレイン間のチャネルとなり，ソース・ドレイン間に電位差を与えるとチャネルを伝わってソースからドレインへ電子が流れる．この反転層に対してホール効果を起こし MOSFET をホール素子として利用する．MOSFET を用いた磁気センサの構造を Fig.1 に示す．

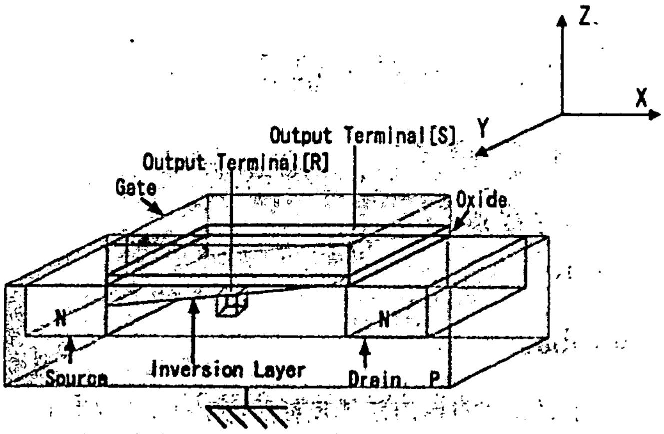

Fig.1 Hall magnetic sensor using channel of n-type MOSFET

Fig.1 のX軸マイナス方向へ電流[I]を流し，Z軸マイナス方向へ磁束[B]をかけるとY軸方向へローレンツ力[F]が発生する．それにより，反転層を流れる電子がローレンツ力によってY軸方向へ曲げられながら進むため Fig.1 の端子[R]と端子[S]間に電位差が生じ，電界が発生する．このホール効果により発生する電位差がホール電圧 V_H であり，式(1)に表される．また，R_H はホール係数，d は反転層の厚さである．

$$V_H = \frac{R_H \cdot I \cdot B}{d} \qquad (1)$$

2.2.読み出し回路とチップ構成

1 つの磁気センサに対する出力電圧の読み出し回路を Fig.2 に示す．2 つの端子からの出力をそれぞれ p チャネル MOSFET, n チャネル MOSFET のソースフォロアで増幅し，ボルテージフォロアでインピーダンスを変換して 20 倍の差動増幅にかけ出力電圧として測定する．また，V_{pb} と $V_{nb}1$, $V_{nb}2$ はソースフォロアのアクティブロードへのバイアスである．

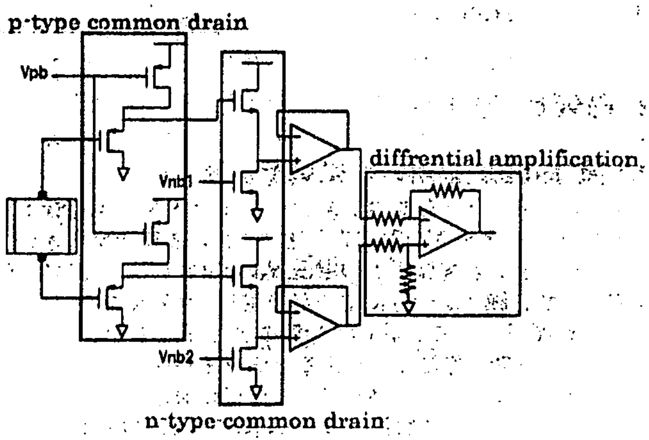

Fig.2 Read-Out Circuit

チップは，ROHM 社の 0.35μm 標準 CMOS プロセスルールで製作された 2 層ポリ 3 層メタル構造である．チップサイズは 4.9mm□であり，そのうち 3.2mm□がセンシングエリアとなっていて，50μm□の磁気センサが 64×64 のアレイ状に配置されている．また，磁気センサの右端の 2 列がホール素子の構造を変化させた TEG を配置した．Fig.3 に磁気センサチップの写真と直径 5mmΦ長さ 5mm の磁石を右上隅に近づけた二次元磁束分布図を示す．

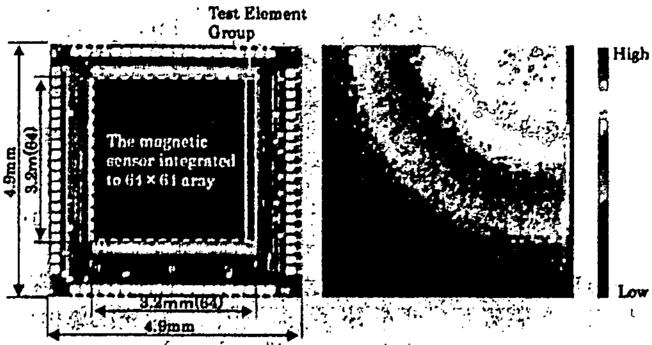

Fig.3 Fabricated LSI chip and two-dimensional magnetic field distribution.

3.ダイナミックドライブ方式

ダイナミックドライブ方式が従来のスタティックドライブ駆動と異なるのは，スタティックドライブ駆動が常時すべてのセンサが ON になっている状態であるのに対し，ダイナミックドライブ駆動は読み出す行だけをだけ駆動させて消費電力を抑えることができる点である．この駆動方式により消費電力が大幅に減らす事ができる．これにより，従来のチップより大きい電流を流すことができるため，ノイズなどの影響を受けにくくなると考えられる．3 行駆動のダイナミックドライブ駆動の例を Fig.4 に示す．

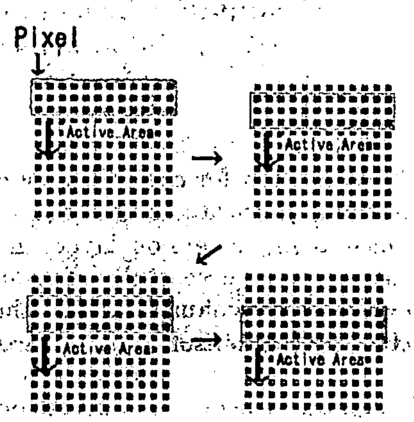

Fig.4 Dynamic drive method

4.試作チップ測定結果

実験では精度の高い位置計測を行えるように磁石を 10μm 単位で移動，固定できる測定器を使用して行った．測定に使用した磁石は直径 1mmΦ長さが 10mm，磁石とセンサ表面との距離が 0.2mm の状態で測定を行った．この時の磁束の強さは 0.55T である．磁石の固定位置はセンシングエリアの中心である．

実験の方法は，まず水平読み出しクロックの周波数を 2MHz から 7.5MHz まで 0.5MHz ずつ順に上げていき，磁束分布図を読み出す速度の限界値を測定した．測定した二次元磁束分布図と周波数の関係を Fig.5 に示す．Fgi5 の括弧内の数値は読み出し速度であり，単位は frame/sec である．

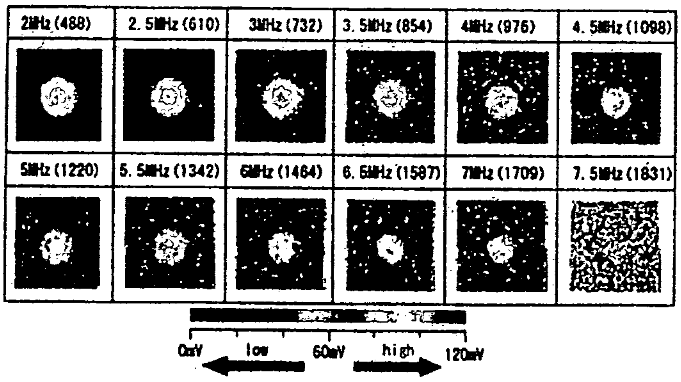

Fig.5 Frequency characteristics of magnetic field

Fig.5 の実験結果から 3MHz(732frame/sec)の読み出し速度からノイズが出ているが，目標としていた 4MHz(1000frame/sec)以上の読み出し速度でも円形の磁束分布図を得られることが確認できた．

次に磁束分布図を用いた位置計測の精度と読み出し速度の関係を調べた。それぞれの周波数で測定した磁束分布図を元にプログラムで磁石の位置を算出した結果を Fig.6 に示す。

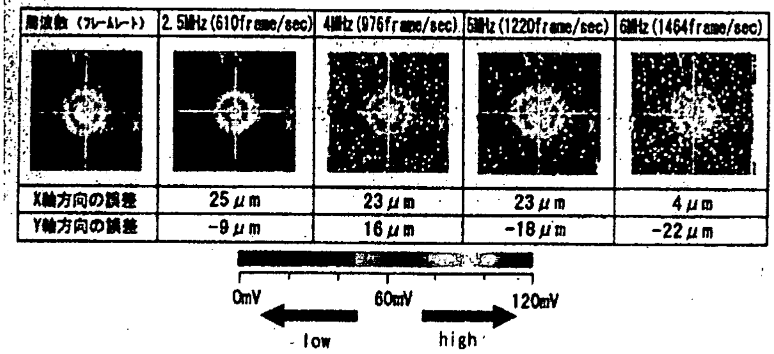

周波数（フレームレート）	2.5MHz(610frame/sec)	4MHz(976frame/sec)	5MHz(1220frame/sec)	6MHz(1464frame/sec)
X軸方向の誤差	25μm	23μm	23μm	4μm
Y軸方向の誤差	-9μm	16μm	-18μm	-22μm

Fig.6 Accuracy measurement of position detection

Fig. 6 の結果から 6MHz(1464frame/sec)で読み出した磁束分布図に対して位置計測を行った場合でも±25μm以下の精度で磁石の位置の同定を行うことができた．しかし，ノイズが多いことから誤差が大きくなってしまう問題が残った．

5.電子の分布

ソースからドレインへ電子が流れる間，ローレンツ力[F]はかかり続けるのでドレインに近づくほど電子は曲げられながら進む．よって，ソース近傍とドレイン近傍とで電子の分布に偏りがあると予想される．

また，ドレイン電圧を高めることによりドレイン側の反転層が途切れるピンチオフが起こる．電子は電界によってソースからドレインへ進むが，反転層が途切れているところは空乏層になっており，強力な電界がかかる．それにより，電子の挙動が異なるため端子[R]，端子[S]の位置によって出力されるホール電圧 V_H が変化する可能性がある．よって，端子の位置を変更した素子で出力電圧の測定を行い，評価した．電子分布の偏りのイメージを Fig.7 に示す．Fig.7 は Fig.1 中のソース，ドレイン，反転層の一部を上から見た図である．

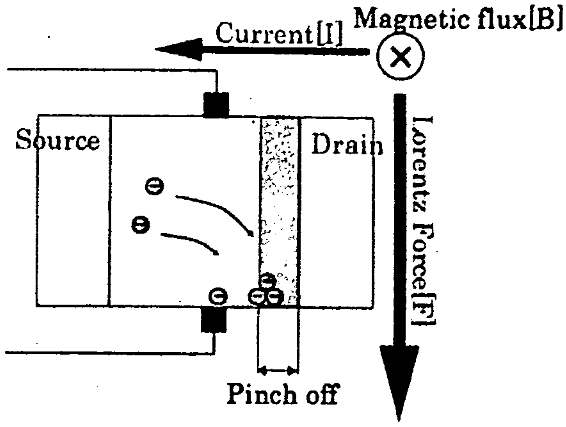

Fig.7 Image of electric distribution

6.素子の構造

6.1.変更端子位置

Fig.8 に左側をソース，右側をドレインとし，変化させた端子位置を示す．従来の端子位置である④から 1.2μm ずつそれぞれの端子を平行にずらし測定を行った．

また，1 個の磁気センサ内のホール素子は 13.2μm 角であり，電圧を読み取る出力端子の幅は 0.6μm である．

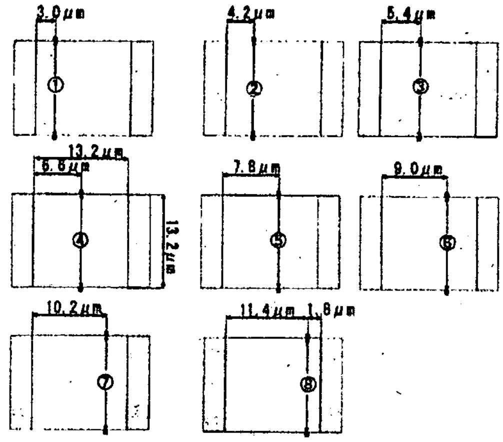

Fig.8 Detail of contact-position

6.2.二次元磁束分布図による比較

Fig.3 中の二次元磁束分布図の右上隅をを拡大した図を Fig.9 に示す．Fig.9 中の点線枠内に Fig.8 の端子位置の磁気センサが配置されている．

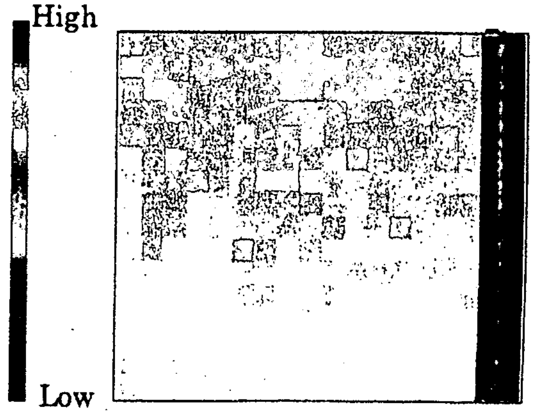

Fig.9 Expansion of two-dimensional magnetic field distribution

Fig.9 から平行に端子位置をずらした磁気センサが従来の端子位置の磁気センサと比べ出力電圧が大きく変化していることが確認できる.

6.3.出力電圧評価

Fig.8 に示したパターンのうち①, ②, ④, ⑦, ⑧の磁束密度に対する出力電圧の測定結果を Fig10 に示す. Fig.10 から端子位置を変更した磁気センサは磁束密度に対して線形に出力電圧が変化していることがわかる. よって, 端子位置を変更した磁気センサは出力電圧向上に利用できると言える.

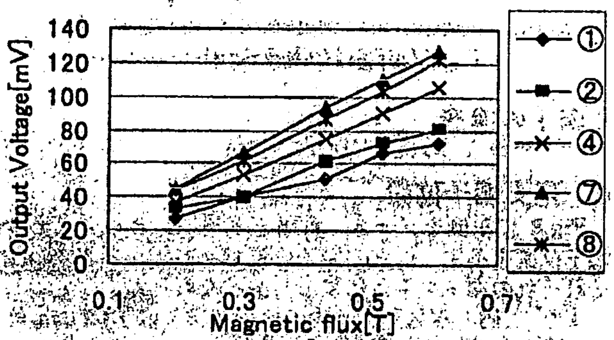

Fig.10 Magnetic flux – Output voltage

従来の端子位置である④に対する各端子の出力電圧比及び標準偏差を Table.1, Fig.11 に示す. Table.1, Fig.11 からドレイン寄りの端子位置である⑦, ⑧において約 20%の出力電圧向上が見られ, 標準偏差は④と比較してもなんら遜色ない.

Table.1 Output voltage ratio at each terminal position

	平均電圧[mV]	増幅率[%]	2ρ[mV]
①	54.15	55.71	7.20
②	70.47	73.02	10.64
③	85.25	88.84	11.09
④	96.82	100.00	10.02
⑤	104.51	109.74	10.75
⑥	110.88	115.05	12.51
⑦	117.32	119.68	10.74
⑧	117.26	119.13	10.16

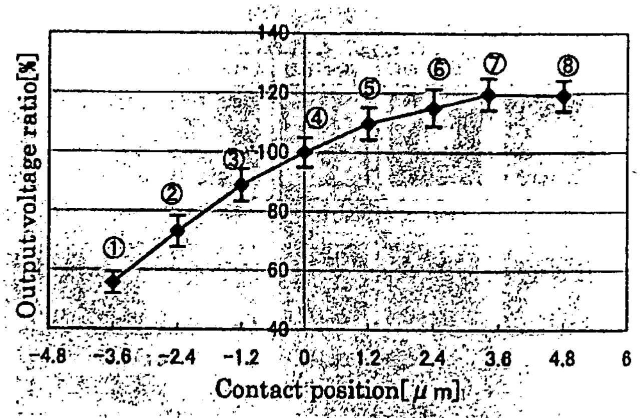

Fig.11 Output voltage ratio at each terminal position

7.まとめ

本研究では, MOS 構造を利用した集積化磁気センサについて検証を行った.

ダイナミックドライブ方式を導入し, 1 つの磁気センサの駆動力を増加させた結果, 位置測定の誤差を 1 画素(±25μm)以内でモーターの制御に必要とされる 1000frame/sec の読み出し速度を達成した.

端子位置を変更した磁気センサで測定を行った結果, 端子位置をドレイン近傍へ変更することで最大約 20%の出力電圧向上が可能であることがわかった.

謝辞

本研究の一部は厚生労働科学研究費補助金によって行われた. 本チップ試作は東京大学大規模集積システム設計教育研究センターを通し, ローム株式会社, 凸版印刷株式会社, ケイデンス株式会社およびシノプシス株式会社の協力で行われたものである.

参考文献

[1]R.V.GALLAGHER and W.S.CORAK
"A METAL-OXIDE-SEMICONDUCTOR(MOS) HALL ELEMENT",
Solid-State Electronics, Vol.9, 1966, pp.571-580.

Collagen-phospholipid polymer hybrid gel designed for artificial blood vessel

Kwangwoo Nam[1], Tsuyoshi Kimura[1], Toshiya Fujisato[2], Takeshi Nakatani[2], Soichiro Kitamura[2], Akio Kishida[1,2].
[1]Division of Biofunctional Molecules, Institute of Biomaterials and Bioengineering,
Tokyo Medical and Dental University
2-3-10 Kanda-Surugadai, Chiyoda-ku, Tokyo 101-0062, JAPAN
[2]National Cardiovascular Center
5-7-1 Fujishiro-dai, Suita, Osaka 565-8565, JAPAN
TEL: 03-5280-8029 FAX: 03-5280-8005 E-mail: bloodnam.fm@tmd.ac.jp.

Introduction: Collagen is often applied for diverse biomaterial, especially for cell related products, for its many advantages. However, use of collagen should be considered very carefully for its high thrombogenicity and low mechanical strength [1]. In order to use collagen as a artificial blood vessel, prevention of graft failure resulting from thrombus formation, and reinforcement of physical and mechanical properties is required. 2-methacryloyloxyethyl phosphorylcholine (MPC)-collagen network gel was developed. MPC polymer is a well-known material for its blood compatiblity and being applied in biomaterial field in various form [2]. In this study, we prepared a collagen hybrid gel using MPC polymer and collagen by immobilizing MPC polymer on the collagen gel surface and characterized the physical properties of this gel.

Methods: Collagen was made into film and was cross-linked by immersed into the 0.05M 2-morpholinoethane sulfonic acid (MES) buffer (pH 9) *N*-(3-dimethylaminopropyl)-*N'*-ethylcarbodiimide (EDC) and *N*-hydroxysuccinimide (NHS) for 4 hours at 4°C. And then this gel was immersed into MES buffer containing EDC/NHS-preactivated poly[2-methacryloyloxyethyl phosphorylcholine (MPC)-*co*-methacrylic acid] (PMA) and immobilized PMA on the collagen gel to make a collagen hybrid gel. To increase the mole ratio of PMA immobilized on the collagen, EDC/NHS activated PMA was re-added to the collagen hybrid gel and immobilized under same condition as written above to make a double-immobilized collagen hybrid gel (DIC hybrid gel). X-ray photoelectron spectroscopy (XPS) and Scanning electron microscope (SEM) was used to characterize the surface of the hybrid gel. Swelling ratio and free amine group analysis was used to characterize the cross-linking efficiency. Collagenase was used to measure the stability of collagen hybrid gel against degradation. And cell adhesion test was executed to characterize the cell compatibility of the collagen hybrid gel.

Results / Discussion: PMA was successfully immobilized on the surface of the collagen gel. XPS result showed that the phospholipids group was mainly deposited on the surface of the collagen gel. And when the surface morphology and the razor-cut surface was observed by SEM, the surface became much smooth compared to that of uncross-linked surface. The razor-cut surface showed that the porous layer, indicating collagen layer, was placed between non-porous layers of PMA. This implies that the collagen hybrid gel would be phase separated, with PMA layer totally covering the collagen gel.

The free amine groups exist in the microfibrils was about 60%. The percentage of unreacted amine group decreased maximum 20% when the gel is cross-linked once again by same procedure. The cross-link of the collagen gel using EDC and NHS is known stop reacting after 1 hour [3], but the re-activation of carboxylic group by EDC and NHS made the collagen to cross-link with PMA and formed much denser network.

The shrinkage temperature increased for the collagen hybrid gel compared to uncross-linked collagen gel. This implies that immobilization of PMA occurred on the surface of the collagen gel, but made the gel tougher and protect the gel from the thermal degradation by forming much denser network. Formation of the denser network increased the elastic modulus also.

The collagen gel would be completely degraded by collagenase within 3 hours. In the case of collagen hybrid gel, approximately 40% would be degraded after 3days. And for DIC gels, it would be left undegraded for more than a week. The leak of PMA was not detected, for DIC gel, indicating that the high cross-link network would be stable.

The contact angle of the collagen gel decreases as the PMA is immobilized on the collagen. The surface of the gel is turning hydrophilic, indicating that the surface is becoming more blood compatible and able to control the cell adhesion. The cell adhesion test using L929 showed that the number of cell adhered on the surface decreases as the density of PMA increased. This is not due to the toxicity, for phospholipids polymer is already proven to be non-toxic [4]. The morphology of the cells was round, indicating the interaction between the cell and surface was suppressed. This result was also observed by other groups [5].

Conclusions: The collagen that was immobilized on the collagen gel was firmly cross-linked with collagen microfibrils. The adoption of phospholipids polymer increased the mechanical property, while maintaining its soft tissue viscoelastic behavior. Increase in the hydrophilicity made the cell difficult to adhere, which is the affect of phospholipid head group.

References: [1] M. J. B. Wissink *et al., Biomaterials* **22** (2001) pp. 151-163. [2] K. Ishihara, *Sci Technol Adv Mater* **1** (2000) pp.131-138. [3] L.H.H. Olde Damink *et al., Biomaterials* 17 (1996) 765-773. [4] T. Ito et al., Collo Surf B Biointerf **41** (2005) 175-180. [5] A. Yamasaki et al., Coll Surf B Biointerf **28** (2003) 53-62.

P1

Influence of nano-vibration stimuli on cell differentiation for tissue engineering

TK Kimura[1], YI Ito[1], TF Fujisato[2], TM Masuzawa[3], AK Kishida[1]
[1]Tokyo Medical and Dental University, TOKYO, Japan
[2]National Cardiovascular Center Res. Ins, OSAKA, Japan
[3]Ibaraki University, HITACHI, Japan

The handling of cells is one of important factors for tissue engineering. Recently, physical stress and stimuli, such as 2-D stretch, hydrostatic pressure and shear stress, have been extensively studied for controlling cell function. In this study, we report the influence of nano-vibration stimuli as physical stress on cell differentiation. Here, we adopted nano-vibration stimulation system as a novel physical stimulation method. The piezo-electric actuator is employed to apply micrometer- to nanometer amplitude. To investigate the influence of nano-vibration on cell differentiation, PC12 cells were used as model cell and stimulated using nano-vibrator. The cells were seeded on multi culture plate and then nerve growth factor (NGF) was added at final concentration of 50 ng/ml. The cell culture plate was set on nano-vibrator and shaken at various frequencies for 1 hour from day to day. The morphology of live cells was observed by light microscope for 4 days. The cells having at least one neurite with a length equal to the cell body diameter were defined as differentiated cells. The degree of cell differentiation was expressed as a percentage of the total cells. In the case of no addition of NGF, the cells were hardly differentiated with and without nano-vibration stimuli. On the other hand, with NGF, the cell differentiation was observed and promoted with nano-vibration in the initial stages. The length and number of neurite per a cell were investigated using NIH image. The no different in number and length of neurite was observed with or without nano-vibration stimuli. These findings may lead to novel cell culture systems controlling cell differentiation of some of stem and progenitor cells.

P29

Development of bioscaffold preserving collagenic structure in biological tissue

DT Terada[1], K Sawada[2], H Ogata[1], K Yoshida[3], S Funamoto[4], T Fujisato[1], A Kishida[4], N Nagaya[1], T Nakatani[1], S Kitamura[1]
[1]National cardiovascula center, SUITA-CITY OSAKA, Japan
[2]Osaka Seikei College, OSAKA, Japan
[3]Found for Biomed Res & Innovation, KOBE, Japan
[4]Tokyo Medical & Dental Univ, TOKYO, Japan

The development of regenerative vascular grafts is strongly desired especially for the pediatric patients. There are many research works related to artificial grafts made of biodegradable synthetic materials. However, it is still difficult to control the biodegradability due to their hydrolysis, adapt the mechanical properties required in the artery, and reproduce complex shape such as aortic arch. In this study, a regenerative collagenic vascular graft was developed from porcine aorta by removing cells and structural proteins other than collagen from the tissue.
Porcine aorta was isolated from the Clawn miniature pig (Japan Farm, Co. Ltd.). The tissue was placed in a vacuum oven at 120·C to cross-link collagen fibers. Elastin fibers were then taken away form the tissue by enzymatic digestion using elastase of 0.56 u/ml in tris buffer solution including $CaCl2$ of 10 mM and $NaN3$ of 0.02% at 37·C with gentle stir. The obtained tissue was subjected to histological and biomechanical studies.
The mechanism of cross-linking by the dehydrate heat treatment in vacuum atmosphere may be attributed to condensation reaction between a carboxyl or hydroxyl group and an amino group of the protein. However, the elastic fibers were digested enzymatically even after the treatment and it was confirmed histologically that the obtained tissue has no elastic fiber and cellular components inside. The collagen fibers remaining in the tissue were also degraded completely by collagenase. The tensile strength certainly decreased after the enzymatic treatment, however an appropriate cross-linking could reduce the decline in tensile strength. The tensile strengths of the obtained vascular graft, a porcine native aorta, and pulmonary artery were 1.09, 2.45, and 0.87 MPa, respectively. The graft may applicable not only to the pulmonary artery but to the other arteries. Also, the graft may have better ability to promote cell infiltration and tissue remodeling compared with the acellular tissue without elastin digestion since the tissue may have more porous structure. The original structure was well preserved all through the process.
The collagenous grafts were prepared by the cross-linking followed by elastin digestion of the porcine vascular tissue. This may be adapted to the vascular tissue regeneration.

(42) Cell Culture on Nano-Vibrating Surface for Controlling Cell Function

Ito Y., Kimura T., Higami T., Fujisato T., Kato A., Masuzawa T., Kishida A.

Tokyo Medical and Dental University, Institute of Biomaterials and Bioengineering, Tokyo, Japan
Sapporo Medical University, Sapporo, Japan Osaka Institute of Technology, Osaka, Japan
Ibaraki University, Ibaraki, Japan

Introduction: Handling cell function is one of important factors for preparing functional cell groups. Recently, physical stress, such as hydrostatic pressure and shear stress, has been studied for controlling cell function. These systems are inspired by physiological stress. To examine the influence of non-physiological stress on cell function, we developed nano-vibration system. In this study, we report the effect of nano-vibration stimuli on cell function–cell adhesion, proliferation and differentiation.

Methods: To investigate the influence of nano-vibration on cell adhesion and proliferation, L929 cell and MEF were used as typical cells. In the differentiation experiment, PC12 cell was used. All cells were vibrated at 10 kHz for 1 hour everyday for 4 days. Then, the alternation was studied by counting cell number, observation of cell shapes and gene expression analysis using real-time RT-PCR.

Results: In L929 cell, there was no effect of nano-vibration on adhesion and proliferation. On the other hand, MEF cell showed drastic change in adhesion and proliferation by nano-vibration. PC12 cell was hardly differentiated without nerve growth factor (NGF) addition, irrespective of nano-vibration. On the other hand, with NGF, the cell differentiation was promoted by nano-vibration in early culture period. However, the level of integrin and neuritin gene expression was not different in both nano-vibration and static culture.

Conclusion: We found that nano-vibration was effective on cell adhesion, proliferation and differentiation. These findings may lead to novel cell function controlling systems for stem and progenitor cells.